

Article

A Comprehensive Study on the Serbuoys Offshore Wind Tension Leg Platform Coupling Dynamic Response under Typical Operational Conditions

Zhe Ma ^{1,2}, Nianxin Ren ^{1,2}, Yin Wang ^{1,*} , Shaoxiong Wang ², Wei Shi ^{1,2}  and Gangjun Zhai ^{1,2}

¹ State Key Laboratory of Coast and Offshore Engineering, Dalian University of Technology, Dalian 116024, China; deep_mzh@dlut.edu.cn (Z.M.); rennianxin@dlut.edu.cn (N.R.); weishi@dlut.edu.cn (W.S.); zhai@dlut.edu.cn (G.Z.)

² Deepwater Engineering Research Centre, Dalian University of Technology, Dalian 116024, China; 787927942@mail.dlut.edu.cn

* Correspondence: y.wang@dlut.edu.cn

Received: 9 April 2019; Accepted: 28 May 2019; Published: 30 May 2019



Abstract: A new type of offshore wind tension leg platform (TLP) connected with a series of buoys (Serbuoys-TLP) is proposed. With the consideration of coupling effect, derivations on the stiffness of the Serbuoys-TLP mooring lines are given. The complicated coupling motion characteristics of the TLP with buoys system are investigated by means of experiments and numerical analysis. The suppressive efficiency on the surge under some condition is nearly 68%, when the wave period is the common wave period of the East China Sea (6 s). Namely, the suppressive effect of series buoys on surge motion response of TLP is analyzed. Through several aspects of suppressive effect on the surge including wave properties, submerge volume and position of buoys are investigated. The modal analysis method is also adopted to interpret the coupled motion response. In the end, the responses of TLP and Serbuoys-TLP are simulated under actual sea conditions with the consideration of wind, wave and current. Based on the parametric study using the modal analysis combined with hydrodynamic analysis, the conclusion can be drawn that the surge of TLP can be effectively suppressed by the addition of a series of buoys in the Serbuoys-TLP.

Keywords: offshore wind turbines; Serbuoys-TLP; stiffness derivations; mode analysis; wind-wave-current combined effect

1. Introduction

Wind energy has the advantages of the lowest environmental impacts, and high cost efficiency and sustainability. Wind energy contributed almost 34% of the total newly installed renewable energy capacity in 2016 [1] and the generation of wind energy experienced a rapid growth during the past ten years worldwide [2]. Especially, the exploitation of offshore wind energy has become an important development direction of wind energy industry [3]. As the design water depth of offshore wind farms is becoming deeper and deeper, the foundation of offshore wind turbine (OWT) is changing from the traditional fixed-bottom type to innovative floating type, which might be more suitable and more potentially economical for deep water [4].

Floating foundations are deeper water substructures that aim to harness better wind resources in further out open seas. The floating offshore wind turbine (FOWT) consists of a floating platform and a mooring system connecting to the seabed. The most representative one is the “Hywind” in Norway, which is the first floating offshore wind turbine project in the world [5]. The tension leg platform (TLP) because of its excellent performance, has gradually become an important type of structure of developing deep-sea wind resources [6].

The U.S. National Renewable Energy Laboratory (NREL) proposed the concept of a tension-leg-type FWT in 2005 and compared it with the other wind turbines [7]. Matha et al. comprehensively investigated the dynamic performance of a 5 MW tension-leg-type FOWT in 2009. This study confirmed the advantage of tension leg platform foundations in FWT applications [8]. Zhao et al. [9] preliminarily designed a multi-column TLP foundation for a 5-MW offshore wind turbine. Studies of the mini tension-leg platform have also greatly promoted the development of tension-leg-type FOWTs and also provide some important methods for analyzing the motion performance of the FOWTs equipped with tension-legs [10,11]. Therefore, during the past decade, more attention has been focused on the design of new TLP concepts to improve the performance of tension-leg-type FOWTs like the tension and energy efficiency.

Ren et al. [12] proposed a tension-leg platform type floating offshore wind turbine system based on the 5 MW offshore wind turbine model. To improve the performance of the TLP system, one tentative strategy of adding mooring lines to the TLP system was proposed, and the force levels of tension legs were effectively reduced. Oguz et al. [13] described an experimental and numerical investigation of the Iberdrola TLP wind turbine concept in realistic wind and wave conditions. The results from studies showed the benefits of such TLP structures in terms of motions which are vital to obtain a high power output from a floating offshore wind turbine.

Nevertheless, the central feature for TLP is that restraining freedom in vertical plane with tension tendons making it similar to a rigid body, while for the horizontal plane, the constraint is less, making it similar to a compliant body [14]. Having an in depth view of the structural response of a TLP is an important issue, not only for response analysis but also for engineering design [15]. It has previously been observed in other studies that the motion of TLPs is large in the horizontal plane [16]. Although many researchers have done conceptual designs before, there is little published data on new tension leg conceptual designs to overcome the problem in the horizontal plane caused by this characteristic.

Therefore, in this study, a new type of tension-leg-type wind turbine connected with a series of buoys (Serbuoys-TLP) is proposed to improve the motion performance of tension-leg-type FOWTs in the horizontal plane. The coupling effects of the Serbuoys-TLP system are investigated by conducting both numerical analysis and model tests. The higher-order boundary element method is adopted to solve the boundary value problem in which multi-body hydrodynamic interactions is treated as generalized mode approach [17]. Modal analysis is also an important means of interpreting dynamic responses [18]. To investigate the characteristics of the Serbuoys-TLP, the modal analysis of the Serbuoys-TLP had been conducted on the commercial software platform ANSYS. The results measured in frequency and time domain analyses showed good agreements with the results of the modal analysis. Finally, the simulation of Serbuoys-TLP wind turbine under typically actual sea condition has been carried out with the consideration of winds, waves and currents. The results indicate that the Serbuoys-TLP wind turbine has a better performance in the horizontal plane compared with tradition tension-leg-type FOWT.

2. Numerical Model of the Serbuoys-TLP System

The Serbuoys-TLP system has been modeled as two rigid bodies: a TLP type FOWT and a series buoys connected tension leg in Figure 1 [12]. Hydrodynamic properties and the coupling interaction effects of the two rigid bodies involved in the Serbuoys-TLP system have been simulated based on AQWA code in the frequency domain and the time domain, which is flexible for modeling multi-body systems and can accommodate the introduction of both mechanical and hydrodynamic couplings between two bodies, and aerodynamic loads on the wind turbine rotor are simplified as equivalent thrusts and bending moments (with the user-force function of AQWA code) based on the design data of the NREL 5 MW wind turbine [8].

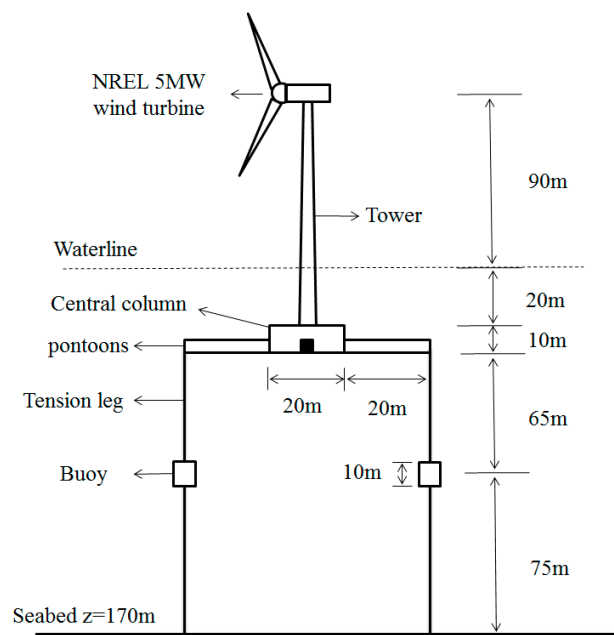


Figure 1. Sketch map of the Serbuoys-TLP concept system.

2.1. Governing Equation in Frequency Domain

Frequency domain analysis is not only the basis of hydrodynamic analysis, but also the premise of the time domain analysis [19]. The equation of motion is as follows:

$$[-\omega^2(M_s + M_a) - i\omega(B_v + B_t) + (K + C)]x = F_{ex} \quad (1)$$

where M_s is the structure mass, M_a is the added mass, B_v is the viscous damping, B_t is the mooring damping, K is the mooring stiffness, C is the restoring force of stillness water, F_{ex} is the wave force.

The damping matrix (no radiation damping) and surge stiffness are obtained in next section, and these values should be added to the corresponding card of ANSYS-AQWA to obtain relatively accurate results.

2.1.1. Mooring Stiffness Matrix of Serbuoys-TLP in Surge and Sway Direction

The mooring stiffness matrix of traditional tension leg foundation have the same form as Serbuoys-TLP as shown in Equation (2). The derivation process of TLP is described by Chandrasekaran [20]. With the consideration of coupling effect, derivations on the stiffness of the Serbuoys-TLP mooring lines are given (see Section 2.3):

$$K = \begin{bmatrix} K_{11} & 0 & 0 & 0 & 0 & 0 \\ 0 & K_{22} & 0 & 0 & 0 & 0 \\ K_{31} & K_{32} & K_{33} & K_{34} & K_{35} & K_{36} \\ 0 & K_{42} & 0 & K_{44} & 0 & 0 \\ K_{51} & 0 & 0 & 0 & K_{55} & 0 \\ 0 & 0 & 0 & 0 & 0 & K_{66} \end{bmatrix} \quad (2)$$

2.1.2. Vicious Damping of Serbuoys-TLP

Based on the linear formula of drag force, the viscous damping can be estimated by a Fourier series expansion [21]:

$$F_d \approx \frac{4}{3\pi} \rho C_d A V_a |V_a \cos \omega t| = B_v |V_a \cos \omega t| \quad (3)$$

where V_a is the velocity amplitude of structure at frequency ω , A is the motion amplitude, and C_d has a value of 0.7.

2.2. Governing Equation in Time Domain

2.2.1. Motion Response Analysis of the Wind Turbine's Upper Platform

It is relatively straightforward to simulate complex nonlinear coupling motions of multi-body systems with complex mooring arrangement and many other external forces, including nonlinear effect when utilizing the time domain simulation [22]. To find the nonlinear mooring force of tendons G , each buoy force are integrated into the entire tension leg. G is introduced into the motion equation of the Serbuoys-TLP wind turbine and the motion response in the time domain is calculated, as shown in the Equation (4):

$$(M + m)\ddot{v} + B\dot{v} + Kv = F + G \quad (4)$$

where M and m are the mass and added mass matrix, v is the displacement. B is the damping matrix. K is the stiffness matrix, F is the applied loading and G is the mooring force of the tendon.

2.2.2. Analysis on Motion Response of Additional Buoy

Assume the tension of a series of buoy upper and lower ends is provided by the upper and lower parts of the tendon, and the pull action line of the nodes coincides with the buoy axis. The buoy model can then be simplified as shown in Figure 2. In time domain analysis, the buoy force equilibrium equation with tension leg and TLP platform effect can be expressed as follows:

$$G_B + F_B + T_{Pu} + T_{Pl} + F_{Pi} + F_{Pf} = 0 \quad (5)$$

The center of gravity (COG) of the series of buoys is located geometrically centered, and the local coordinate system located in the COG. At the beginning, the local coordinate system in the positive direction with the same global coordinate system. The displacement of the local coordinate system can be obtained by calculation, the angle of the local coordinate system can be determined though the relative spatial relationship between the buoy upper and lower nodes [23]. The forces acting on the buoy include gravity G_B , buoyancy force F_B , pull force provided by the buoy upper and lower nodes T_p , T_{pb} , inertial force F_{pl} , drag force (considering the relative velocity between buoy and water particles) F_{pf} . The balance equation is shown as Equation (5).

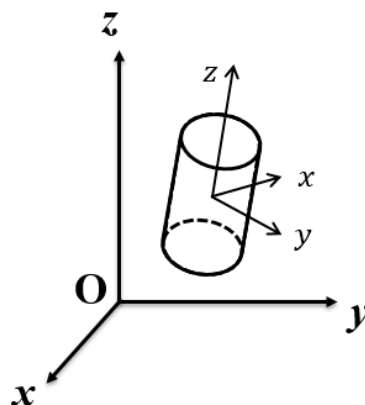


Figure 2. Coordinate systems of buoys.

2.3. Mooring Stiffness of the Serbuoys-TLP System

A single tendon is studied in this section, as shown Figure 3. In order to calculate the mooring stiffness of a Serbuoys-TLP system, the buoy can be simplified as a buoyancy point. The tendon

is truncated by the buoy, and the stiffness of each segment is performed based on static analysis. The following variables can be assumed to solve the mooring stiffness.

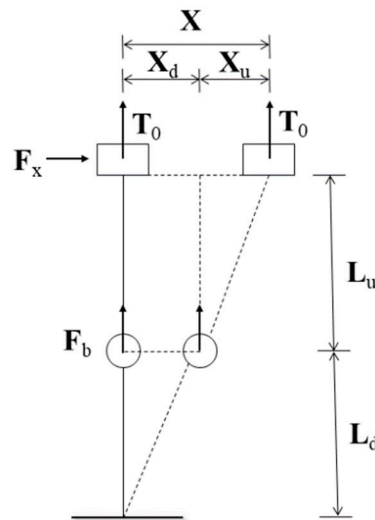


Figure 3. Force diagram of tendons with series connected buoy.

T_0 and F_b are the initial pre-tension in the tether and buoys, respectively. When the platform produces a unitary horizontal displacement x under the action of horizontal force F_x . L_{u0} and L_{d0} are the original length of the upper and lower tendon, ΔL_u and ΔL_d represent the elongation when the tendon has been installed. $\Delta L'_u$, $\Delta L'_d$ and x_u , x_d represent the elongation with the tendon has been installed and the horizontal displacement of the upper and lower tendon when the platform has produced a horizontal displacement, respectively. H is the vertical distance from the center of platform gravity to the mooring point. A_t is the cross-sectional area of the tether, and E is Young's modulus of the tether. There are three relationships between these above physical quantities:

$$\begin{cases} L_u = L_{u0}(1 + T_0/EA_t) \\ L_d = L_{d0}(1 + (T_0 + F_b)/EA_t) \end{cases} \quad (6)$$

$$\begin{cases} \Delta L_u = L_{u0}T_0/EA_t = L_u - L_{u0} \\ \Delta L_d = L_{d0}(T_0 + F_b)/EA_t = L_d - L_{d0} \end{cases} \quad (7)$$

$$\begin{cases} \Delta L'_u = \sqrt{x_u^2 + L_u^2} - L_u \\ \Delta L'_d = \sqrt{x_d^2 + L_d^2} - L_d \end{cases} \quad (8)$$

Because x_u and x_d are the unknown quantity, a new equilibrium equation (Equation (6)) must be added. The horizontal forces at the top and bottom of the buoy are the same:

$$k_{11u}x_u = k_{11d}x_d = k_{11}x = F_x \quad (9)$$

where k_{11} is the surge stiffness for one tendon, and k_{11} can be rewritten as:

$$k_{11} = \frac{T_0 + \Delta T_h}{L + \Delta L_h} \approx \frac{T_0}{L} \quad (10)$$

where ΔT_h and ΔL_h are the variation of tension and length due to the arbitrary displacement given in the surge degree of freedom.

It can be seen from Equations (9) and (10), $x \propto L/T$, thus:

$$x_u \frac{T_0}{L_u} = x_d \frac{T_0 + F_b}{L_d} \quad (11)$$

Considering x contains x_u and x_d , so:

$$x_u = \frac{L_u(T_0 + F_b)}{L_u(T_0 + F_b) + L_d T_0} x \quad (12)$$

$$x_d = \frac{L_d T_0}{L_u(T_0 + F_b) + L_d T_0} x \quad (13)$$

$\Delta L'_u$ and $\Delta L'_d$ can be calculated when Equations (12) and (13) are brought into Equation (8). Based on Hooke's law, the upper and lower section surge stiffness of the tendon are written as follows:

$$k_{11u} = \frac{T_0 + \Delta T_{1u}}{L_u + \Delta L'_u} \quad (14)$$

$$k_{11d} = \frac{T_0 + F_b + \Delta T_{1d}}{L_d + \Delta L'_d} \quad (15)$$

By the series theorem of rigidity:

$$K = \frac{k_1 k_2}{k_1 + k_2} \quad (16)$$

so, the surge stiffness of a single tendon can be deduced as follows:

$$k_{11} = \frac{(T_0 + \Delta T_{1u})}{(L_u + \Delta L'_u) + (L_d + \Delta L'_d) \frac{(T_0 + \Delta T_{1u})}{(T_0 + F_b + \Delta T_{1d})}} \quad (17)$$

The total surge stiffness of the Serbuoys-TLP system is four times as much as that of a single tendon. When the horizontal displacements is assumed to be a small quantity, there is:

$$K_{11} = \frac{4T_0}{(L_u + L_d) - L_d F_b / (T_0 + F_b)} \quad (18)$$

$K_{21} = 0$, as no force develops in the sway direction when an arbitrary displacement occurs in the surge direction.

Equilibrium of forces in the heave direction gives:

$$k_{31u} = \frac{4}{L_u x_u} (EA_t \Delta L'_u - T_0 \Delta L_u) \quad (19)$$

$$k_{31d} = \frac{4}{L_d x_d} [EA_t \Delta L'_d - (T_0 + F_b) \Delta L_d] \quad (20)$$

$$K_{31} = 4k_{31} = 16 \frac{(EA_t \Delta L'_u - T_0 \Delta L_u) [EA_t \Delta L'_d - (T_0 + F_b) \Delta L_d]}{L_d x_d (EA_t \Delta L'_u - T_0 \Delta L_u) + L_u x_u [EA_t \Delta L'_d - (T_0 + F_b) \Delta L_d]} \approx 0 \quad (21)$$

$K_{41} = 0$, as no moment develops along the roll direction when an arbitrary displacement occurs in the surge direction.

Summation of moments along the pitch direction gives:

$$K_{51} = -HK_{11} = \frac{-4HT_0}{(L_u + L_d) - L_d F_b / (T_0 + F_b)} \quad (22)$$

$K_{61} = 0$, as no moment develops along the yaw direction when an arbitrary displacement occurs in the surge direction.

3. Description of Physical Model Test

The scale model tests of the Serbuoys-TLP system have been done in the advanced wave flume laboratory located at the Harbin Institute of Technology (HIT). The numerical model is validated against the model test. Comprehensively considering the condition of the laboratory and the size of full-scale Serbuoys-TLP system, the scale ratio of the Serbuoys-TLP test model has been designed to be 1/50 with Froude's law. The overall view of the main combined structure system and locations of installed sensors for monitoring main dynamic responses of the Serbuoys-TLP system are shown in Figure 4. The scale model is mainly based on the scaling law of the similarity of Froude numbers. The scale test model is mainly made of organic glass, and the main design parameters of which are listed in Table 1.

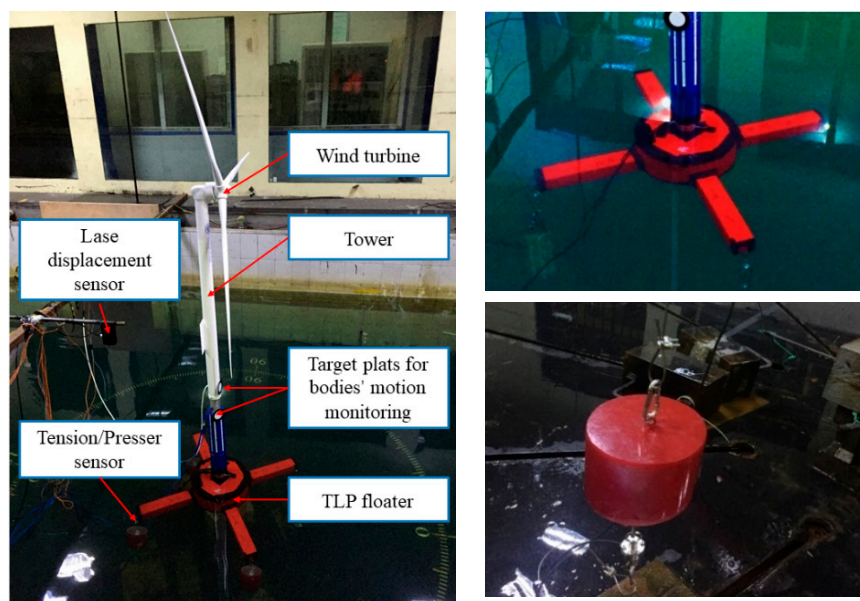


Figure 4. Scale model test system.

Table 1. Main design parameters of the Serbuoys-TLP model.

Parameters	Full Scale	Scaled $\lambda = 1/50$
NTEL 5 WM Wind turbine		
Blades and Nacelle mass (kg)	350,000	2.80
Tower mass (kg)	350,000	2.80
Tower Height (m)	90	1.80
TLP platform		
Buoyancy (kg)	5,214,000	41.71
Total mass (kg)	2,814,000	22.51
Water depth (m)	170	3.40
Center of gravity (m)	(0, 0, -1.0)	(0, 0, -0.02)
Cylinder buoy size (m)	R = 10.0; H = 10.0	Ra = 0.20; Ha = 0.20
$I_{xx} \approx I_{yy}$; I_{zz} (kg·m ²)	4.5×10^9 ; 5.0×10^8	14.40; 1.6
Pontoon design (m)	L = 20.0; A = 4.0 × 4.0	L = 0.40; A = 0.08 × 0.08
Tension leg (m)	L = 70; D = 1.2; t = 0.04	Equivalent steel cable
Serbuoys		
Serbuoys Diameter (m)	D = 5.6; H = 10	Da = 0.112; Ha = 0.2
Serbuoys Buoyancy (kg)	250,000 × 4	2 × 4

The six-DOF motions of the Serbuoys-TLP have been tracked by a stereovision measurement system with two high-quality cameras and target plates, and for details of the working principle readers can refer to reference [12]. Considering the surge response is the most significant motion for the TLP system, an additional laser displacement sensor has been used for measuring the surge displacement of the TLP platform (assisting the stereovision measurement system).

The tension leg system in the model test has been simplified as four steel cables (stiffness equivalent to tension legs in the prototype). There is a waterproof tension sensor (with a sensitivity of 0.01 N) at the top of each tension leg to measure tension responses of each tension leg. The bottom ends of the four tension legs are connected to four heavy plates to simulate the TLP foundation.

To make sure the data sampling is synchronized, the laser displacement sensor, the stereovision measurement system, accelerometers sensor, tension/pressure sensors have been all set to record data at the same time with the same sample frequency of 100 Hz during model tests. In addition, the stereovision measurement system and waterproof tension sensors have all been calibrated before doing model tests.

4. Results and Discussion

The experimental results were compared with the results from the numerical analysis. To investigate the multi-body effect of buoys thoroughly, both the frequency and time domain analysis were performed. The numerical model is shown in Figure 5. The parameters of buoys are consistent with the prototype in Table 1 and the buoys are installed at 95 m underwater.

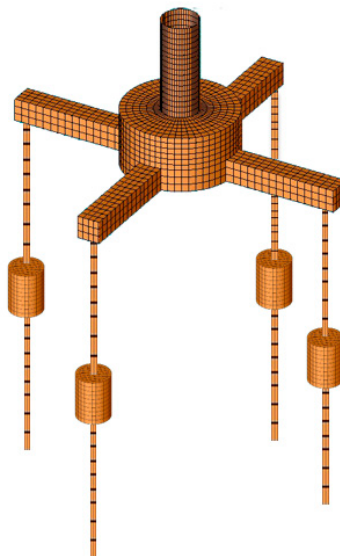


Figure 5. Panel model of Serbuoys-TLP system for the hydrodynamic analysis.

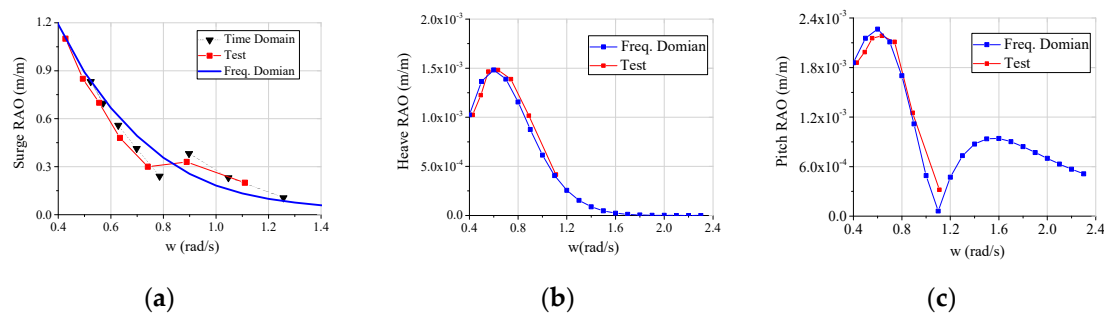
4.1. Validations on the Serbuoys-TLP

Typical free decay tests have been done both in model tests and numerical simulations to identify natural periods by the numerical simulations are used to compare with those measured data from the model test. Main results are listed in Table 2. Due to the symmetry of the structure, the yaw response is small and the yaw period is ignored. It can be seen that numerical results have a good agreement with the experimental measurements, although the numerical results have very small relative differences. The surge response is of great importance in designing a TLP type floating system. Therefore, it is thoroughly investigated throughout the present study and also used to validate our numerical model.

Table 2. Main natural period results of the Serbuoys-TLP system.

	Simulation (Ts)	Test (Tt)	Relative Difference (Ts - Tt)/Tt
Surge/Sway (s)	30.2	32.1	−5.91%
Heave (TLP) (s)	0.65	0.68	−4.41%
Pitch/Roll (s)	0.74	0.78	−5.13%

Furthermore, the motion response amplitude operator (RAO) of the Serbuoys-TLP systems is determined and acquired from a regular wave test and analysis both with frequency domain and time domain, shown in Figure 6. Due to the limitations of the experimental conditions, we only compare the results of frequency 0.4–1.1 rad/s in experiments with the frequency/time domain results. From Figure 6a, it can be seen that the time domain results have a better agreement with the test data than those in the frequency domain analysis, although the time domain model seems to slightly overestimate the dynamic responses of the Serbuoys-TLP system without accounting for the viscous damping effect in the scale test model. Especially at the high frequency, there is a resonance frequency although the surge RAO of it is small. It should be noted that this wave frequency belongs to the common range of wave frequency under the water depth in the simulation, so it should be discussed in detail. While this phenomenon is not observed in frequency domain, we adopt the time domain simulation in following the comparison between the TLP and Serbuoys-TLP. However, the typical responses of the TLP can be observed in Figure 6a–c and the resonance frequencies of all motions are consistent with those obtained by the free decay tests. For the vertical motions, heave and pitch exhibited the resonance at the wave frequency. Its responses are much smaller than horizontal motion. Therefore, the vertical motions are ignored in following discussion.

**Figure 6.** Dynamic responses analysis of the Serbuoys-TLP system under typical regular wave test conditions. (a) Surge; (b) Heave; (c) Pitch.

4.2. Comparison of Serbuoys-TLP and TLP

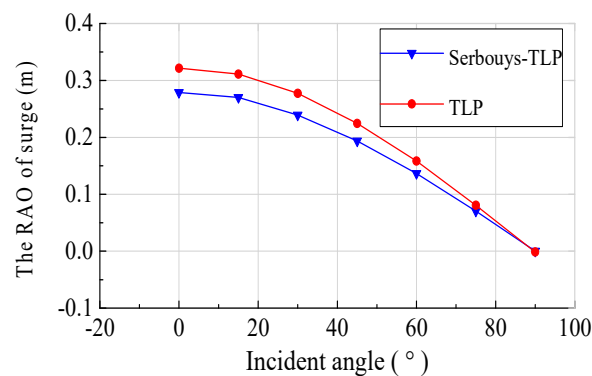
To examine the influence on the suppressive effect in the numerical simulations, the working conditions are divided into two groups, considering the variable and fixed two kinds of factors on the suppressive effect. Namely, group one consisting of A, B and C; other one of D, E and F. A total of 60 operating cases under various working conditions are modelled and they are listed in Table 3. As in Section 4.1, the average value of motion amplitude under each working condition in time domain is displayed in the form of RAO. The time domain simulation model of TLP is exactly same as that of Serbuoys-TLP, except that there is no buoy on the tension leg.

Table 3. Working condition settings.

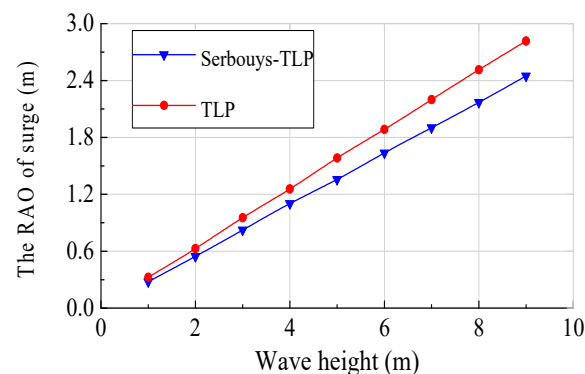
Work Condition	Incident Wave Direction/ $^{\circ}$	Wave Height/m	Wave Period/s
A (7 cases)	0;15;25;45;60;75;90	1	10
B (9 cases)	0	1;2;3;...;7;8;9	10
C (11 cases)	0	1	3;4;5;...;11;12;15
Work condition	Position of buoy/m	Total displacement of buoys/t	Water depth/m
D (11 cases)	-60	1000	170
E (11 cases)	-95	1000	170
F (11 cases)	-95	2000	170

4.2.1. Effect of Wave Parameters on the Surge Suppressive Effect of a Series of Buoys

The working condition of A, B, C correspond to wave incidence angle, wave height and wave period, respectively. The effects of these three working conditions are respectively shown in Figure 7. As seen in Figure 7a, the surges of both Serbuoys-TLP and a typical TLP decrease as the incidence angle increases. For all the incidence angles, the surges of the Serbuoys-TLP are lower than those of the typical TLP. When examining the effect of wave height on the surge (see Figure 7b), both structures exhibit a rising tendency with the wave height. Similarly, the Serbuoys-TLP shows a good ability to suppress the surge over the typical one.



(a)



(b)

Figure 7. Cont.

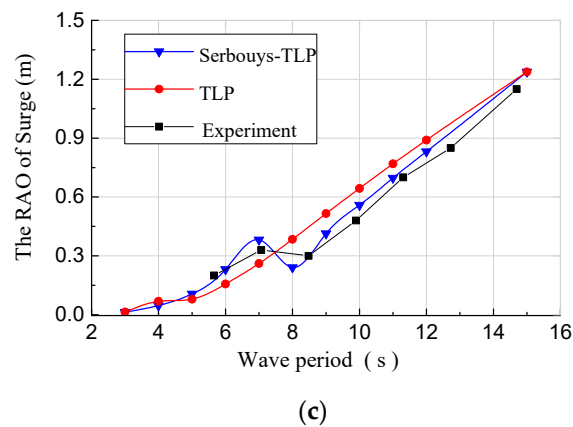


Figure 7. Surge contrast of TLP and Serbuoys-TLP under working condition A, B and C. (a) Condition A; (b) Condition B; (c) Condition C.

Figure 7c shows that the RAO of TLP and Serbuoys-TLP surge in working condition C increases with the increase of wave period. The experimental results for wave periods of 5.66 s, 7.07 s, 8.48 s, 9.90 s, 11.31 s, 12.73 s, and 14.70 s, are in good agreement with the numerical results. The surge motion of Serbuoys-TLP displays a peak at a wave period of about 7 s. Before the peak, the suppressive effect on the surge of TLP is not ideal, and the surge of the Serbuoys-TLP is even larger than that of TLP. After the peak, the suppressive effect of the series buoy on the surge decreases with the increase of the wave period and the best suppressive efficiency is about 36.62%. This is mainly because the buoys on the tension leg alter the natural frequencies of the TLP when the buoys and platform are coupled. The frequency of incident wave coincide with the higher natural frequencies of the Serbuoys-TLP, resulting in resonance. However, this resonance period belongs to the common period of wave, so more attention should be paid this phenomenon in the design and application of Serbuoys-TLP. Next, we will discuss the influence of buoy parameters on the suppressive effect and this resonance peak value. The suppressive efficiency of motions (Λ) under the working conditions A and B is expressed by:

$$\Lambda = (A_{\text{TLP}} - A_{\text{Serbuoys-TLP}})/A_{\text{TLP}} \quad (23)$$

here A_{TLP} is the surge amplitude of TLP under a certain regular wave condition; $A_{\text{Serbuoys-TLP}}$ is the surge amplitude of the Serbuoys-TLP system under a certain regular wave condition. The suppressive efficiency under working conditions A and B is summarized in Table 4.

Table 4. The suppressive efficiency of a series of buoys to surges under working conditions A and B.

Working Condition	Suppressive Efficiency	Working Condition	Suppressive Efficiency
A ($\theta = 0^\circ$)	13.24%	B (H = 2 m)	12.96%
A ($\theta = 15^\circ$)	13.21%	B (H = 3 m)	13.82%
A ($\theta = 30^\circ$)	13.75%	B (H = 4 m)	13.21%
A ($\theta = 45^\circ$)	13.73%	B (H = 5 m)	13.48%
A ($\theta = 60^\circ$)	13.89%	B (H = 6 m)	13.29%
A ($\theta = 75^\circ$)	12.72%	B (H = 7 m)	13.01%
A ($\theta = 90^\circ$)	–	B (H = 8 m)	13.28%
B (H = 1 m)	12.86%	B (H = 9 m)	13.10%

When the suppressive efficiency is bigger than zero, the Serbuoys-TLP has a lower surge response with a good performance. The higher the suppressive efficiency is, the better the Serbuoys-TLP performs compared with the typical TLP. Under both working conditions A and B (corresponding respectively to wave incidence angle and height), the suppressive effect of the Serbuoys-TLP is very convincing, with an efficiency of about 13%. It should be noted that when the wave incidence angle is

90, the efficiency is not meaningful since there is no any surge for either the Serbuoys-TLP or the typical TLP with a wave incidence perpendicular to the surge direction. In general, the new Serbuoys-TLP shows a good suppressive effect performance over q typical TLP with suppressive efficiencies higher than zero in all the cases.

4.2.2. Buoy Parameter on the Suppressive Effect of a Series of Buoys

When the displacement and position of the buoys change, it often causes a change of the structure natural frequency, therefore affecting the result of the surge response on the Serbuoys-TLP. The displacement and the position of buoys connected the tension leg are discussed under the working conditions of group D, E, F.

For a case where there is a resonance intent, which is characterized by a peak followed by a trough, the suppressive effect is usually evaluated by the value of RAO under a specific wave period after a resonance intent. From Figure 8, it is seen that the post-resonance intent RAO values are relatively lower for the low series buoys position (case D) than those for the high series buoys position (case E). This implies that low-position series buoys have a good suppressive effect performance. Through examining the wave period at which a resonance intent occurs, it is found that the resonance occurs at a smaller wave period for the low-position series buoys, while the high-position one corresponds to a big wave period. It is also seen that the post-resonance intent RAO values are relatively lower for the heavy series buoys displacement (case F) than those for the light series buoys displacement (case E). This implies that heavy-displacement series buoys have a good suppressive effect performance. It is very meaningful in practical design to improve the suppressive effect by adjusting the series buoys displacement and position according the local wave conditions. It is clearly seen that the suppressive effect performance is improved by adding the series of buoys when comparing with the typical TLP without a series of buoys.

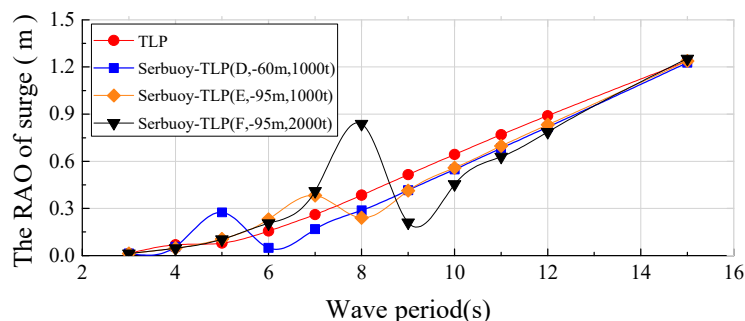


Figure 8. Surge contrast of TLP and Serbuoys-TLP under working conditions D, E and F.

4.3. Mode Analysis

To interpreted the coupling resonance phenomenon of the Serbuoys-TLP system, mode analysis is usually adopted in practical design [24]. The mode analyses for the group D, E, F have been performed. A total of 12 mode shapes were examined and they are summarized in Table 5. It can be clearly seen that the first half-wave period of the Serbuoys-TLP under the conditions D, E and F are near 5 s, 7 s and 8 s, respectively. This is a very good explanation for the resonance phenomenon in noted the previous section. When the wave period is in this resonance range, the motion of the Serbuoys-TLP will increase significantly. The maximum half-wave period of TLP is about 3 s beyond the common wave range so that there will be no the resonance phenomenon in the small wave periods compared with Serbuoys-TLP.

Table 5. Natural periods of the TLP type wind turbine.

Mode#n	TLP	D	E	F	Remarks
1	34.56	32.31	32.62	33.24	Surge mode
2	34.56	32.31	32.61	33.24	Sway mode
3	18.23	19.18	18.17	19.49	Yaw mode
4	3.23	5.05	6.88	8.74	Tether mode-1h
5	3.23	5.04	6.88	8.74	Tether mode-1h
6	3.23	5.03	6.77	8.74	Tether mode-1h
7	3.23	5.03	6.77	8.74	Tether mode-1h
8	3.22	5.02	6.77	8.73	Tether mode-1h
9	3.19	4.73	6.68	8.33	Tether mode-1h
10	3.19	4.72	6.68	8.33	Tether mode-1h
11	3.11	4.07	5.99	7.31	Tether mode-1h
12	1.55	2.00	1.50	1.71	Tether mode-2h

In this paper, four modes of traditional TLP and Serbuoys-TLP (Case E) wind turbines are given, respectively. The modal shapes of modal numbers 1, 3, 9 and 12 are shown in Figures 9 and 10, respectively. The mode shapes of group D and F are basically the same as those of group E. From the results, it can be seen that the period corresponding to tether mode-1h decreases with the increase of buoy position. When the period is less than 5 s, a Serbuoys-TLP structure with excellent hydrodynamic performance can be obtained. However when the location of the buoys is higher, it will be subjected to wave loads, thus increasing the motion response. Although increasing the displacement of buoys can improve the stiffness of mooring system, resonance phenomena will occur in more common sea conditions wave periods. Therefore, the design parameters of the series of buoys, namely, the position and displacement, ought to be selected based on the results by combing the mode and hydrodynamic analysis.

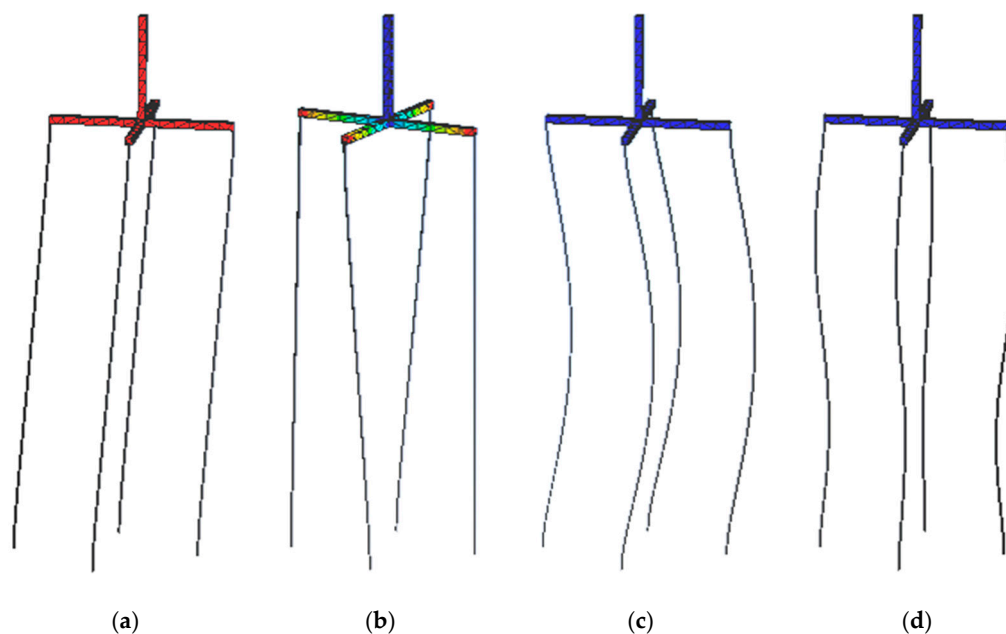


Figure 9. Mode shapes of TLP. (a) $n = 1$ (Surge); (b) $n = 3$ (Yaw); (c) $n = 9$ (Tether-1h); (d) $n = 12$ (Tether-2h).

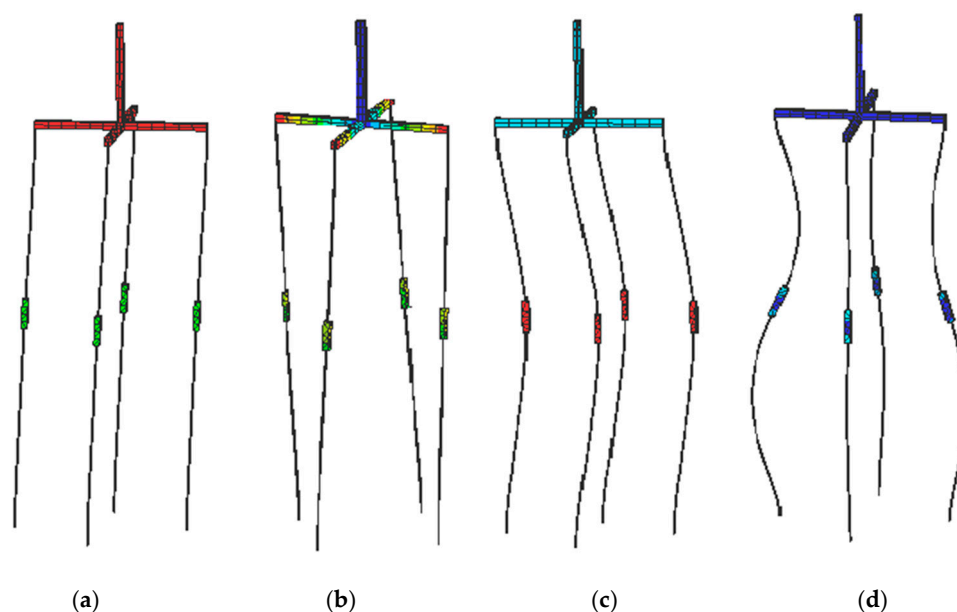


Figure 10. Mode shapes of Serbuoys-TLP. (a) $n = 1$ (Surge); (b) $n = 3$ (Yaw); (c) $n = 9$ (Tether-1h); (d) $n = 12$ (Tether-2h).

4.4. Wind-Wave-Current Coupling Effect

In the real ocean environment, the Serbuoys-TLP structure is often subjected to winds, waves and currents at the same time. In this section, the coupling effect is analyzed by considering the wind, wave and current loading conditions. The numerical model of the tension leg floating wind turbine is the same as that introduced with the basic parameters listed in Table 1. The environmental parameters of wind, wave and current are considered in the present analysis and listed in Table 6.

Table 6. Environmental parameters of typical sea conditions in China.

Significant wave heights H_s/m	2.4
Spectral wave peak period T_p/s	13.4
Wind speed (average one hour)/ $m \cdot s^{-1}$	11.4
Surface current velocity/ $m \cdot s^{-1}$	0.6

The 5 MW wind turbine model proposed by the U.S. National Renewable Energy Laboratory (NREL) is adopted in the simulation [8]. The wind loading force is set up in the model by defining the time spectrum of wind speed associated with the wind speed (see Figure 11a) in accordance with the RP 2 SK specification and further obtained by looking up the relationship of the horizontal wind force and wind speed curve (see Figure 11b) [25]. The frequency spectrum of the wind speed is obtained and shown in Figure 11c. By doing so, the impulse features of the wind load can be described in the numerical model with advantage over the typical loading way using a constant wind load. This loading treatment is able to better reflect the real conditions. The current load is adding using a uniform current speed profile with depth to the numerical model and taken into account as a constant force converted in the standard way of the API RP 2SK. In our numerical model, the wave load is defined by adopting a Jonswap spectrum with two characteristic parameters of significant wave heights and spectral wave peak period. The most unfavorable direction of the three-type loads to which the projection of the series buoys has the maximum area, is considered in the numerical simulations.

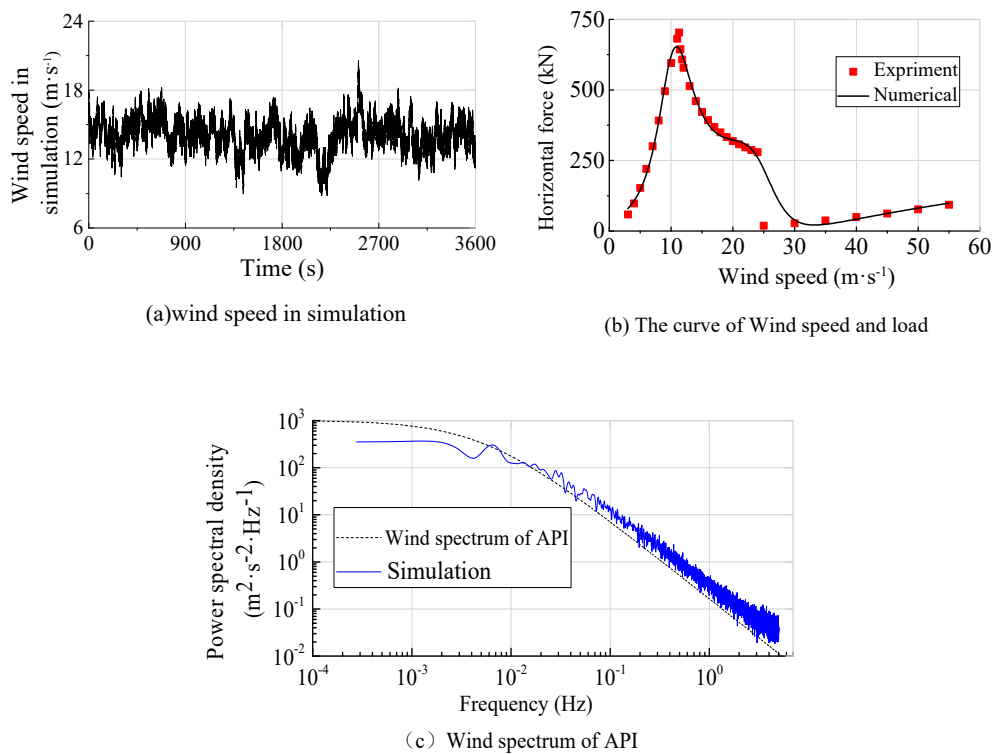


Figure 11. Relationship between horizontal wind load and wind speed and API wind in Simulink.

A progress of 3600 s is simulated by our numerical model and the relationships between the surge and time are shown in Figure 12. It is clearly seen that the Serbuoys-TLP exhibits significantly lower surges than those of the typical TLP. By adding the series of buoys, the TLP performs very well in the suppressive effect aspect. For the Serbuoys-TLP, lower surges can be predicted when a non-uniform current speed profile with the depth, like happens in real conditions [26,27], is considered in the numerical model. It is expected that the new type of Serbuoys-TLP can show its further suppressive effect potential.

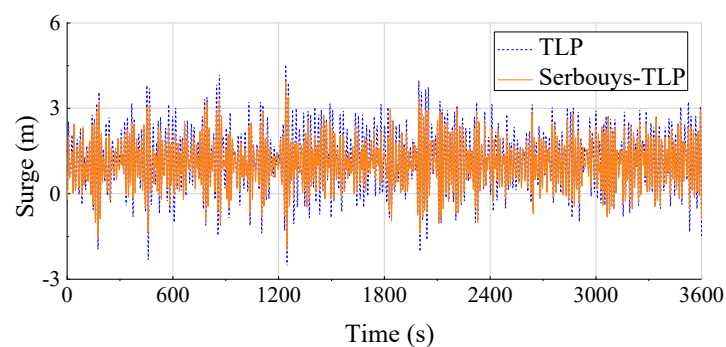


Figure 12. Surge response time history curve of wind turbines under the working sea state.

5. Conclusions

This paper proposes the concept of a new type of tension-leg-type wind turbine connected with a series of buoys (Serbuoys-TLP). The complicated coupled motion characteristics of the TLP with a buoy system are investigated by means of experimental and numerical analysis. In the numerical approach, both frequency and time domain approaches have been applied. In the frequency domain, the mooring stiffness matrix of the Serbuoys-TLP is derived for accurate and efficient calculation of coupled mooring forces. The time domain simulation is applied with consideration of nonlinear factors

between platform, tendon and buoys with nonlinear wave forces. The complex behaviors of time domain analysis are identified from modal analysis which is also a meaningful method for practical application of Serbuoys-TLP. From the systematic comparison between model tests, modal analysis, numerical analyses both in frequency domain and time domain, the following conclusions could be drawn:

- (1) Under the most of the regular wave conditions, buoys attached to tension leg can effectively improve the horizontal motion, especially during surges. A TLP surge suppressive efficiency as high as 60% is seen above under some conditions; In the case of irregular waves, the results show that the buoys can effectively suppress the surge motion response of the TLP, particularly at the peak.
- (2) Wave height and the incidence angle of waves cannot change the suppressive efficiency on the surge of TLP, but it is different from the wave period. The natural frequency of the Serbuoys-TLP has been changed due to the addition of buoys on the tension leg. Therefore, the phenomenon of wave-frequency resonance is captured in both a time domain simulation and experimental tests. On both sides of the resonance period, the suppressive effect is quite different, which needs special attention to avoid wave frequency resonance.
- (3) The position and displacement of the buoys have a great influence on the suppressive effect. Generally speaking, A lower position and the larger displacement of buoys corresponds to a larger resonance period, and the suppressive effect is more obvious after the resonance intent. However, due to the existence of wave-frequency resonance, we can not blindly pursue the suppressive effect. Instead, modal analysis and hydrodynamic analysis should be combined to check the parametera of the buoys to get the best results.

Author Contributions: Conceptualization, Z.M. and N.R.; Software, S.W.; Writing—Original Draft Preparation, Z.M. and Y.W.; Writing—Review & Editing, W.S.; Supervision, G.Z.

Funding: This research was supported by the National Natural Science Foundation of China (Grant NO. 51879035, 51709040), the Fundamental Research Funds for the Central Universities. The financial supports are greatly acknowledged.

Conflicts of Interest: The authors declare no conflict of interest.

References

1. Sağlam, Ü. A two-stage data envelopment analysis model for efficiency assessments of 39 state's wind power in the United States. *Energy Convers. Manag.* **2017**, *146*, 52–67. [[CrossRef](#)]
2. Bevrani, H.; Ghosh, A.; Ledwich, G. Renewable energy sources and frequency regulation: survey and new perspectives. *IET Renew. Power Gener.* **2010**, *4*, 438–457. [[CrossRef](#)]
3. Dinh, V.N.; McKeogh, E. Offshore Wind Energy: Technology Opportunities and Challenges. In Proceedings of the First Vietnam Symposium in Offshore Engineering, Lecture Notes in Civil Engineering, Hanoi, Vietnam, 1–3 November 2018.
4. Wang, X.; Zeng, X.; Li, J.; Yang, X.; Wang, H. A review on recent advancements of substructures for offshore wind turbines. *Energy Convers. Manag.* **2018**, *158*, 103–119. [[CrossRef](#)]
5. Skaare, B.; Nielsen, F.G.; Hanson, T.D.; Yttervik, R.; Havmøller, O.; Rekdal, A. Analysis of measurements and simulations from the Hywind Demo floating wind turbine. *Wind Energy* **2015**, *18*, 1105–1122. [[CrossRef](#)]
6. Bangga, G.; Guma, G.; Lutz, T.; Krämer, E. Numerical simulations of a large offshore wind turbine exposed to turbulent inflow conditions. *Wind Eng.* **2018**, *42*, 88–96. [[CrossRef](#)]
7. Musial, W.; Butterfield, S.; Boone, A. Feasibility of Floating Platform Systems for Wind Turbines. In Proceedings of the 42nd AIAA Aerospace Sciences Meeting and Exhibit, Reno, Nevada, 5–8 January 2004.
8. Matha, D. *Model Development and Loads Analysis of an Offshore Wind Turbine on a Tension Leg Platform with a Comparison to Other Floating Turbine Concepts*; National Renewable Energy Laboratory: Golden, CO, USA, 2009.
9. Zhao, Y.; Yang, J.; He, Y. Preliminary design of a multi-column tlp foundation for a 5-mw offshore wind turbine. *Energies* **2012**, *5*, 3874–3891. [[CrossRef](#)]

10. Bhattacharyya, S.K. Experimental and numerical study of coupled dynamic response of a mini tension leg platform. *Offshore Mech. Arct. Eng.* **2004**, *126*, 318–330.
11. Bhattacharyya, S.K.; Sreekumar, S.; Idichandy, V.G. Coupled dynamics of SeaStar mini tension leg platform. *Ocean Eng.* **2003**, *30*, 709–737. [[CrossRef](#)]
12. Ren, N.; Li, Y.; Ou, J. The effect of additional mooring chains on the motion performance of a floating wind turbine with a tension leg platform. *Energies* **2012**, *5*, 1135–1149. [[CrossRef](#)]
13. Oguz, E.; Clelland, D.; Day, A.H.; Incecik, A.; López, J.A.; Sánchez, G.; Almeria, G.G. Experimental and numerical analysis of a TLP floating offshore wind turbine. *Ocean Eng.* **2018**, *147*, 591–605. [[CrossRef](#)]
14. Zeng, X.H.; Li, X.W.; Liu, Y.; Wu, Y.X. Nonlinear dynamic responses of tension leg platform with slack-taut tether. *China Ocean Eng.* **2009**, *1*, 37–48.
15. Taflanidis, A.A.; Vetter, C.; Loukogeorgaki, E. Impact of modeling and excitation uncertainties on operational and structural reliability of tension leg platforms. *Appl. Ocean Res.* **2013**, *43*, 131–147. [[CrossRef](#)]
16. Jain, A.K. Nonlinear coupled response of offshore tension leg platforms to regular wave forces. *Ocean Eng.* **1997**, *24*, 577–592. [[CrossRef](#)]
17. Choi, Y.R.; Hong, S.Y. An analysis of hydrodynamic interaction of floating multibody using higher-order boundary element method. In Proceedings of the 12th International Offshore and Polar Engineering, Kitakyushu, Japan, 26–31 May 2002.
18. Darvishi, A.S.; Bahaari, M.R.; Moradi, M. Natural frequency of offshore wind turbines on rigid and flexible monopiles in cohesionless soils with linear stiffness distribution. *Appl. Ocean Res.* **2017**, *68*, 91–102. [[CrossRef](#)]
19. Low, Y.M. Frequency domain analysis of a tension leg platform with statistical linearization of the tendon restoring forces. *Mar. Struct.* **2009**, *22*, 480–503. [[CrossRef](#)]
20. Chandrasekaran, S.; Jain, A.K. Dynamic behaviour of square and triangular offshore tension leg platforms under regular wave loads. *Ocean Eng.* **2002**, *29*, 279–313. [[CrossRef](#)]
21. Morison, J.R.; O'Brien, M.P.; Johnson, J.W.; Schaaf, S.A. The force exerted by surface waves on piles. *Trans. Am. Inst. Min. Metall. Eng.* **1950**, *189*, 149–154. [[CrossRef](#)]
22. Choi, Y.; Nam, B.W.; Hong, S.Y.; Jung, D.W.; Kim, H.J. Coupled motion analysis of a tension leg platform with a tender semi-submersible system. *Ocean Eng.* **2018**, *156*, 224–239. [[CrossRef](#)]
23. Sugita, T.; Suzuki, H. A study on TLP hull sizing by utilizing optimization algorithm. *J. Mar. Sci. Technol.* **2016**, *21*, 611–623. [[CrossRef](#)]
24. Hermans, L.; Van der Auweraer, H. Modal testing and analysis of structures under operational conditions: industrial applications. *Mech. Syst. Signal Process.* **1999**, *13*, 193–216. [[CrossRef](#)]
25. Jonkman, J.; Butterfield, S.; Musial, W.; Scott, G. *Definition of a 5-MW Reference Wind Turbine for Offshore System Development*; National Renewable Energy Laboratory: Golden, CO, USA, 2009.
26. Tung, C.C. Peak distribution of random wave-current force. *J. Eng. Mech. Div. ASCE* **1976**, *102*, 575–576.
27. Nguyen, H.X.; Basu, B.; Dinh, V.N. Numerical investigation of wave-current interaction by using smoothed particle hydrodynamics. In Proceedings of the First Vietnam Symposium in Offshore Engineering, Hanoi, Vietnam, 1–3 November 2018.

